Generalized Three-Level Optimal Pulse Patterns With Lower Harmonic Distortion

Annika Birth, *Student Member, IEEE*, Tobias Geyer, *Senior Member, IEEE*, Hendrik du Toit Mouton, *Member, IEEE*, and Martinus Dorfling, *Student Member, IEEE*

***Abstract*—Optimized pulse patterns (OPPs) minimize the harmonic distortions of inductive loads. To simplify the analysis and computation, quarter- and half-wave symmetry is typically imposed. Moreover, for three-level converters, the switch positions are required to be non-negative in the positive half-wave of the fundamental period. This article investigates the impact of these restrictions on the harmonic distortions. By relaxing the symmetry requirements and by allowing also negative switch positions in the positive half-wave of the fundamental period, the current distortions can be reduced by up to one-third compared to the traditional OPP formulation.**

***Index Terms*—Half-wave symmetry, medium-voltage drives, optimized pulse patterns (OPPs), quarter-wave symmetry, synchronous optimal pulsewidth modulation.**

I. Introduction

OPTIMIZED switching signals reduce the harmonic distortions in the converter currents [1] and, thus, reduce the harmonic losses in the load. This is particularly important for high-power converters operating at low switching frequencies. The switching signals can be calculated offline by using either selective harmonic elimination (SHE) or optimized pulse patterns (OPPs).

SHE was first mentioned in 1964 [2]. By setting specific harmonics to zero, an algebraic system of equations is derived, whose solutions are the switching angles. The technique was further developed in [3] and [4], and later became popular for low switching frequency applications. For each modulation index, multiple solutions typically exist. To identify all solutions of the system of equations, the method of resultants can be used as proposed in [5].

The concept of OPPs, also referred to as synchronous optimal pulsewidth modulation, was first published in 1977 [6]. This offline modulation technique minimizes the *entire* (weighted) harmonic content in the switching signal instead of eliminating individual harmonics [7]. To this end, an optimization problem is formulated with a cost function that captures the current distortions. By minimizing the cost function subject to constraints on the fundamental voltage component and the order of the switching angles, an optimal set of switching angles is derived for each modulation index. This optimal solution is typically unique. The comparison of three-level OPPs with the corresponding SHE solutions reveals the superior harmonic performance of the OPPs [8]. The OPP problem formulation was extended to multilevel converters in [9].

In both modulation methods, quarter- and half-wave symmetry is typically imposed on the switching signal. For the SHE problem, the restrictive nature of the quarter-wave symmetry condition was first reported in [10]. Several new solutions emerge for two-, three-, and multilevel switching signals when relaxing quarter-wave symmetry, unattainable for the traditional quarter- and half-wave symmetry problem formulation. Furthermore, the removal of quarter-wave symmetry reduces the overall harmonic distortions in the switching signal for certain half-wave symmetric (HWS) solution sets [11]. The additional relaxation of half-wave symmetry results in an infinite number of solutions [12] in the SHE problem.

Only recently, symmetry relaxation in OPPs has been investigated. In [13] and [14], two-level OPPs with relaxed quarter-wave symmetry are computed, which achieve lower harmonic distortions in the converter current in certain intervals of the modulation range. Two-level pulse patterns with only half-wave symmetry imposed are also beneficial when considering the isotropy properties of an electrical machine. As shown in [15], such OPPs result again in lower harmonic distortions in certain intervals of the modulation range.

Another restriction is commonly made for multilevel switching signals: In the positive half-wave of the fundamental period, only non-negative switch positions are considered and vice versa for the negative half-wave. This results in *unipolar* pulse patterns. The relaxation of this restriction by allowing *multipolar* switch positions has not been studied yet, as the published research on OPPs with relaxed symmetry was done only for two-level pulse patterns, to which this restriction is not applicable. We also consider nonzero initial switch positions, which have not been investigated in the unified SHE approach.

It is often assumed that the traditional OPPs achieve *minimal* harmonic current distortions and that, consequently, no switching pattern exists with lower current distortions. However, the

Manuscript received March 14, 2019; revised May 22, 2019, August 1, 2019, and October 24, 2019; accepted November 5, 2019. Date of publication November 14, 2019; date of current version February 20, 2020. Recommended for publication by Associate Editor Prof. F.-J. Lin. *(Corresponding author: Annika Birth.)*

A. Birth, H. du Toit Mouton, and M. Dorfling are with the Department of Electrical and Electronic Engineering, Stellenbosch University, Stellenbosch 7602, South Africa (e-mail: 21519234@sun.ac.za; dtmouton@sun.ac.za; mddorfling@sun.ac.za).

T. Geyer is with ABB Corporate Research, Baden-Dättwil 5405, Switzerland (e-mail: t.geyer@ieee.org).

Color versions of one or more of the figures in this article are available online at http://ieeexplore.ieee.org.

Digital Object Identifier 10.1109/TPEL.2019.2953819

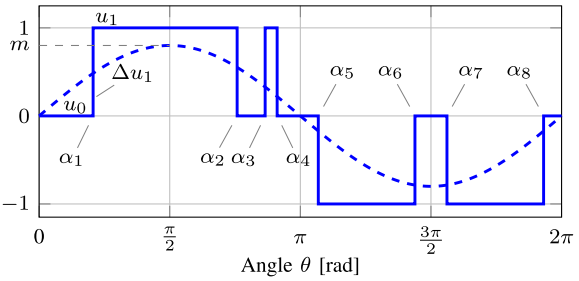

Fig. 1. Single-phase, 2π-symmetric pulse pattern (solid) with $k = 8$ switching angles α_i and switching transitions Δu_i. The pulse number is $d = 2$. The amplitude of the fundamental component (dashed) corresponds to the modulation index m.

typical assumptions on symmetry and polarity of the switch positions impose restrictions on the search space, which can lead to suboptimal results. In this article, these implicitly made restrictions are relaxed, which increases the search space and allows us to find solutions with lower harmonic distortions.

This article is structured as follows. In Section II, the nomenclature is introduced and the objective function is derived. The harmonic analysis of the pulse pattern for different symmetry conditions is presented in Section III, based on which four different optimization problems are derived in Section IV. Section V discusses the resulting OPPs and their harmonic performances, which are experimentally verified in Section VI. Finally, Section VII concludes the article.

II. Optimal Pulse Patterns

We start by defining the pulse number $d = \frac{f_{\text{sw}}}{f_1}$ as the ratio of the *average* semiconductor switching frequency f_{sw} to the fundamental frequency f_1 of the single-phase switching signal. Let k denote the number of switching transitions in one fundamental period. For the three-level neutral-point-clamped inverter, each switching transition corresponds to a turn-on transition in one of the four semiconductor switches in a phase-leg. Within one period, this gives an *average* of $\frac{k}{4}$ turn-on transitions per semiconductor. Thus, the average switching frequency per semiconductor is $f_{\text{sw}} = \frac{k}{4}\, f_1$, resulting in the pulse number $d = \frac{k}{4}$.

Assuming symmetry between the phases, the three-phase switching signal can be constructed from the single-phase switching signal. Therefore, we consider that the single-phase case is sufficient when formulating the OPP problem.

A. Pulse Pattern

We consider a 2π-periodic OPP without any additional symmetry imposed. We refer to this as *full-wave* symmetry. A full-wave symmetric (FWS) OPP with pulse number d is defined by $4d+1$ switch positions u_i with $i \in \{0, \dots, 4d\}$ and $4d$ switching angles α_i with $i \in \{1, \dots, 4d\}$ (see Fig. 1). Due to the 2π-periodicity, the initial switch position matches the last switch position, i.e., $u_0 = u_{4d}$. The ith switching angle corresponds to the ith switching transition $\Delta u_i = u_i - u_{i-1}$. It follows that the ith switch position u_i is given by the sum of the first i switching transitions added to the initial switch position u_0

$$u_i = u_0 + \sum_{j=1}^{i} \Delta u_j. \tag{1}$$

Switching by more than one level up or down is generally prohibited for multilevel inverters; this restricts the switching transitions to $\Delta u_i \in \{-1, 1\}$. Furthermore, for the three-level inverter, the switch positions are restricted to $u_i \in \{-1, 0, 1\}$.

It is clear that the switch positions pose an additional degree of freedom in the optimization problem. Thus, there are two sets of optimization variables: the set of switching angles $\alpha_F = [\alpha_1 \dots \alpha_{4d}]^T$, and the set of switch positions $u_F = [u_0 \dots u_{4d-1}]^T$. Both sets have $4d$ elements.

B. Objective Function

OPPs aim to minimize the harmonic distortions in the inverter output current. To achieve this, the total demand distortion (TDD) of the current is adopted for the objective function in the OPP computation. The current TDD

$$I_{\text{TDD}} = \frac{1}{\sqrt{2} I_{\text{nom}}} \sqrt{\sum_{n \neq 1} \left(\hat{i}_n\right)^2} \tag{2}$$

is the square root of the sum of the squared current harmonic amplitudes $\hat{i}_n$ of order n relative to the nominal (or rated) current, where I_{nom} is the rms value of the nominal current.

Let $\hat{u}_n$ denote the amplitude of the nth harmonic of the single-phase pulse pattern. For a three-level inverter, the amplitude of the corresponding voltage harmonic is $\hat{v}_n = \frac{V_{\text{dc}}}{2} \hat{u}_n$, where V_{dc} is the dc-link voltage.

Assume that the inverter is connected to an inductive load with inductance L_σ. The amplitude of the nth current harmonic directly follows as $\hat{i}_n = \dfrac{\hat{v}_n}{n \omega_1 L_\sigma}$, where $\omega_1 = 2\pi f_1$ denotes the angular fundamental frequency. Note that for an inductive machine, L_σ corresponds to the total leakage inductance. The stator resistance is neglected.

Substituting both mathematical relationships in (2) gives

$$I_{\text{TDD}} = \frac{1}{\sqrt{2} I_{\text{nom}} \omega_1 L_\sigma} \frac{V_{\text{dc}}}{2} \sqrt{\sum_{n \neq 1} \left(\frac{\hat{u}_n}{n}\right)^2}. \tag{3}$$

We interpret (3) as $I_{\text{TDD}} = C\sqrt{J}$. The constant C depends only on the inverter and load parameters, whereas the term

$$J = \sum_{n \neq 1} \left(\frac{\hat{u}_n}{n}\right)^2 \tag{4}$$

is a function of the amplitudes of the switching signal harmonics. Minimizing the current TDD is, thus, equivalent to minimizing J, which is chosen as the general objective function for the OPP optimization problem.

III. Harmonic Analysis of Pulse Patterns

The harmonic distortion of the switching signal can be computed by using a Fourier series expansion. With the assumption

TABLE I
FOURIER COEFFICIENTS a_n AND b_n WHEN IMPOSING FULL-WAVE SYMMETRY, HALF-WAVE SYMMETRY, OR QUARTER- AND HALF-WAVE SYMMETRY ON THE SWITCHING SIGNAL

Full-wave symmetry	$a_n = \begin{cases} 2u_0 - \frac{1}{\pi}\sum_{i=1}^{4d} \Delta u_i \alpha_i, & n = 0 \\ -\frac{1}{n\pi}\sum_{i=1}^{4d} \Delta u_i \sin(n\alpha_i), & n = 1,2,3,\dots \end{cases}$	$b_n = \frac{1}{n\pi}\sum_{i=1}^{4d} \Delta u_i \cos(n\alpha_i), \quad n = 1,2,3,\dots$ (9)
Half-wave symmetry	$a_n = \begin{cases} 0, & n = 0,2,4,\dots \\ -\frac{2}{n\pi}\sum_{i=1}^{2d} \Delta u_i \sin(n\alpha_i), & n = 1,3,5,\dots \end{cases}$	$b_n = \begin{cases} 0, & n = 2,4,6,\dots \\ \frac{2}{n\pi}\sum_{i=1}^{2d} \Delta u_i \cos(n\alpha_i), & n = 1,3,5,\dots \end{cases}$ (10)
Quarter- and half-wave symmetry	$a_n = 0, \quad n = 0,1,2,\dots$	$b_n = \begin{cases} 0, & n = 2,4,6,\dots \\ \frac{4}{n\pi}\sum_{i=1}^{d} \Delta u_i \cos(n\alpha_i), & n = 1,3,5,\dots \end{cases}$ (11)

of 2π-periodicity, the single-phase switching signal is represented by

$$u(\theta) = \frac{a_0}{2} + \sum_{n=1}^{\infty} \big(a_n \cos(n\theta) + b_n \sin(n\theta)\big) \tag{5}$$

with the Fourier coefficients

$$a_n = \frac{1}{\pi}\int_0^{2\pi} u(\theta)\cos(n\theta)\,\mathrm{d}\theta, \quad \text{for } n \geq 0\,, \text{ and}$$
$$b_n = \frac{1}{\pi}\int_0^{2\pi} u(\theta)\sin(n\theta)\,\mathrm{d}\theta, \quad \text{for } n \geq 1\,. \tag{6}$$

The amplitude $\hat{u}_n$ of the nth switching signal harmonic is given by $\hat{u}_n = \sqrt{a_n^2 + b_n^2}$. With this, the objective function (4) becomes a function of the Fourier coefficients

$$J = \sum_{n\neq 1} \frac{a_n^2 + b_n^2}{n^2}. \tag{7}$$

To derive the Fourier coefficients, consider that the switching signal is a piece-wise constant function with $4d+1$ intervals, (see Fig. 1). The integrals of the Fourier coefficients (6) can, thus, be written in $4d+1$ terms of which the limits are the switching angles and the switch positions are a constant factor

$$a_n = \frac{1}{\pi}\left[u_0\int_0^{\alpha_1}\cos(n\theta)\,\mathrm{d}\theta + u_1\int_{\alpha_1}^{\alpha_2}\cos(n\theta)\,\mathrm{d}\theta + \cdots + u_{4d}\int_{\alpha_{4d}}^{2\pi}\cos(n\theta)\,\mathrm{d}\theta\right]. \tag{8}$$

With the help of (1), the switch positions can be represented as the sum of the switching transitions. This allows us to rearrange the integrals as follows

$$a_n = \frac{1}{\pi}\left[u_0\int_0^{\alpha_1}\cos(n\theta)\,\mathrm{d}\theta + (u_0+\Delta u_1)\int_{\alpha_1}^{\alpha_2}\cos(n\theta)\,\mathrm{d}\theta + \cdots + \left(u_0 + \sum_{j=1}^{4d}\Delta u_j\right)\int_{\alpha_{4d}}^{2\pi}\cos(n\theta)\,\mathrm{d}\theta\right] \tag{12}$$

$$= \frac{1}{\pi}\left[u_0\int_0^{2\pi}\cos(n\theta)\,\mathrm{d}\theta + \Delta u_1\int_{\alpha_1}^{2\pi}\cos(n\theta)\,\mathrm{d}\theta + \cdots + \Delta u_{4d}\int_{\alpha_{4d}}^{2\pi}\cos(n\theta)\,\mathrm{d}\theta\right] \tag{13}$$

$$= \frac{1}{\pi}\left[u_0\int_0^{2\pi}\cos(n\theta)\,\mathrm{d}\theta + \sum_{i=1}^{4d}\Delta u_i\int_{\alpha_i}^{2\pi}\cos(n\theta)\,\mathrm{d}\theta\right]. \tag{14}$$

Note that the upper limit of each integral is 2π. Solving the integrals leads to the compact expression in (9) in Table I for the Fourier coefficients a_n of pulse patterns with full-wave symmetry. Similar expressions can be derived for the Fourier coefficients b_n. The FWS pulse patterns consist of harmonics of all orders and different phase shifts, represented by a_n and b_n, as well as the dc-offset a_0.

By imposing half-wave symmetry, the Fourier coefficients depend only on one half-wave of the pattern, as the second half-wave relates to the first one by $u(\pi+\theta) = -u(\theta)$. This eliminates all even harmonics in the switching signal including the dc-offset. The remaining odd harmonics vary in magnitude and phase (see (10) in Table I).

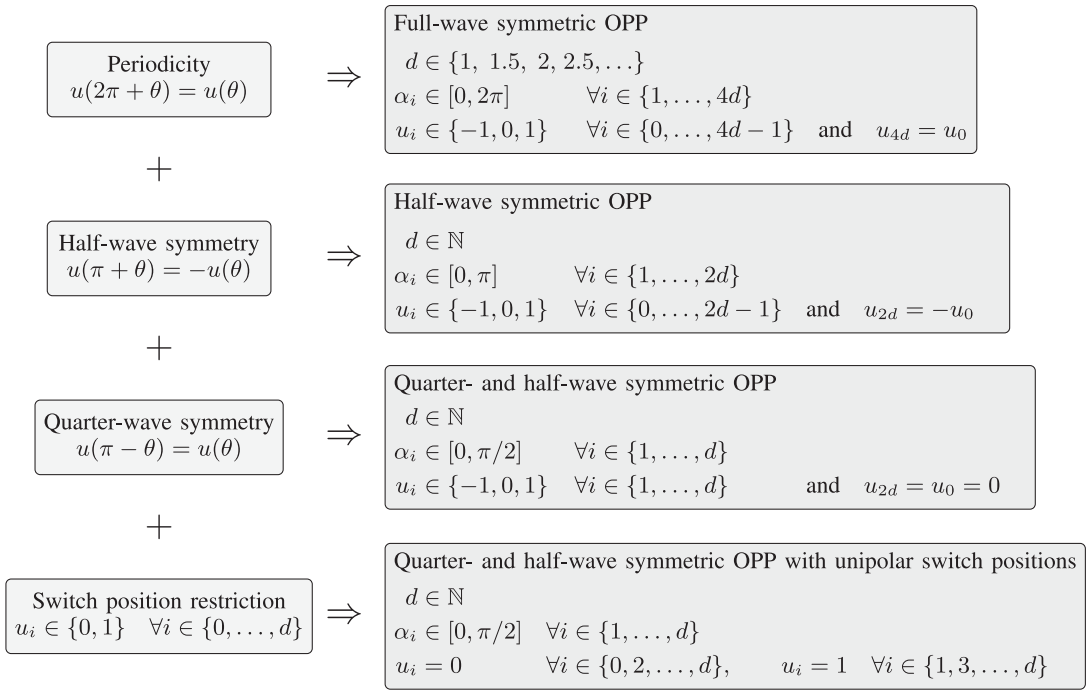

Fig. 2. Overview of the three-level OPP problems, depending on the imposed restrictions of the pulse pattern.

We additionally impose quarter-wave symmetry, i.e., $u(\pi-\theta)=u(\theta)$, on the HWS pulse pattern.[1] The combined quarter- and half-wave symmetry turns the Fourier coefficients a_n to zero (see (11) in Table I). This restricts the phases of the harmonics to 0° and 180°; the magnitudes of the switching signal harmonics are directly given by $\hat{u}_n = b_n$.

For more details on the derivation of the Fourier coefficients when imposing different symmetries, the interested reader is referred to [16]. A detailed derivation of (11) is provided in [17, Ch. 3 Appendix A].

IV. OPP Optimization Problems

The general unrestricted three-level OPP optimization problem with full-wave symmetry and multipolar switch positions is derived. Imposing first half-wave symmetry and, then, quarter-wave symmetry leads to the second and third OPP problems, respectively; both consider multipolar switch positions. Finally, the switch positions are restricted to unipolar values, which yields the traditional OPP problem with quarter- and half-wave symmetry and unipolar switch positions. The characteristics of these four OPP optimization problems are summarized in Fig. 2.

The following three requirements must always be met: the magnitude of the fundamental component must be equal to the modulation index m, where $m \in [0, \frac{4}{\pi}]$, the pulse pattern has a zero dc-offset, and the phase of the fundamental component must be zero.

Consider that third-order voltage harmonics, i.e., integer multiples of three, are in phase. When assuming a symmetric three-phase system with a floating star point, these so-called common-mode harmonics entail no harmonic current. Therefore, only harmonics of nonthird orders, i.e., $n = 2, 4, 5, 7, \ldots$, are considered in the objective function.

A. Full-Wave Symmetry

Assuming 2π-periodicity in the general OPP problem requires $u_{4d} = u_0$; this implies an even number k of switching angles in the pulse pattern. Owing to $d = \frac{k}{4}$, this allows for noninteger pulse numbers $d \in \{1,\ 1.5,\ 2,\ 2.5, \ldots\}$ for FWS OPPs.

With these requirements, the full-wave symmetry optimization problem can be written as

$$\begin{aligned} \underset{\alpha_F, u_F}{\text{minimize}} \quad & J(\alpha_F, u_F) = \sum_{n=2,4,5,7,\ldots} \frac{a_n^2 + b_n^2}{n^2} \\ \text{subject to} \quad & a_0 = 0, \quad a_1 = 0, \quad b_1 = m \\ & 0 \le \alpha_1 \le \alpha_2 \le \ldots \le \alpha_{4d} \le 2\pi \\ & u_i \in \{-1,0,1\} \text{ and } u_{i+1} - u_i \in \{-1,1\} \\ & \forall\, i \in \{0,\ldots,4d-1\} \end{aligned} \tag{15}$$

where $\alpha_F = [\alpha_1 \ldots \alpha_{4d}]^T$ and $u_F = [u_0 \ldots u_{4d-1}]^T$ are the vectors containing the optimization variables, and a_n and b_n are the Fourier coefficients given in (9).

[1] Note that we assume that quarter-wave symmetry and half-wave symmetry are unrelated concepts. For example, pulse patterns with quarter-wave symmetry but without half-wave symmetry can be constructed, e.g., by allowing for a dc offset. For this reason, we distinguish between quarter- and half-wave symmetry, and we define quarter-wave symmetry without the implication of half-wave symmetry.

B. Half-Wave Symmetry

Imposing half-wave symmetry reduces the problem dimension to $2d$ switching angles within $[0, \pi]$, and $2d$ switch positions, where symmetry requires $u_{2d} = -u_0$. This implies an even number of switching transitions within *one half-wave*, i.e., $d \in \mathbb{N}$.

Due to the absence of even harmonics in the HWS pulse pattern, the dc-offset a_0 is always zero (see (10) in Table I). The constraint on the dc-offset can, thus, be dropped and only harmonics of orders $n = 5, 7, 11, \ldots$ are considered in the objective function. This leads to the problem formulation

$$\begin{aligned} \underset{\alpha_H, u_H}{\text{minimize}} \quad & J(\alpha_H, u_H) = \sum_{n=5,7,11,\ldots} \frac{a_n^2 + b_n^2}{n^2} \\ \text{subject to} \quad & a_1 = 0, \quad b_1 = m \\ & 0 \le \alpha_1 \le \alpha_2 \le \ldots \le \alpha_{2d} \le \pi \\ & u_i \in \{-1, 0, 1\} \text{ and } u_{i+1} - u_i \in \{-1, 1\} \\ & \forall\, i \in \{0, \ldots, 2d-1\} \end{aligned} \tag{16}$$

with $\alpha_H = [\alpha_1 \ldots \alpha_{2d}]^T$ and $u_H = [u_0 \ldots u_{2d-1}]^T$.

C. Quarter- and Half-Wave Symmetry

Additionally imposing quarter-wave symmetry restricts the independent switching angles to one quarter of the fundamental period and reduces their number to d. Furthermore, quarter- and half-wave symmetry requires the initial switch position u_0 to be zero.

The Fourier coefficients (11) are zero for even-order harmonics. The phase shifts of the harmonics are either 0° or 180°. As a result, the fundamental component always has zero phase, and the constraint $a_1 = 0$ can be dropped. For quarter- and half-wave symmetry, the OPP problem with $\alpha_Q = [\alpha_1 \ldots \alpha_d]^T$ and $u_Q = [u_1 \ldots u_d]^T$ results in

$$\begin{aligned} \underset{\alpha_Q, u_Q}{\text{minimize}} \quad & J(\alpha_Q, u_Q) = \sum_{n=5,7,11,\ldots} \left(\frac{b_n}{n}\right)^2 \\ \text{subject to} \quad & b_1 = m \\ & 0 \le \alpha_1 \le \alpha_2 \le \ldots \le \alpha_d \le \frac{\pi}{2} \\ & u_i \in \{-1, 0, 1\} \text{ and } u_i - u_{i-1} \in \{-1, 1\} \\ & \forall\, i \in \{1, \ldots, d\}. \end{aligned} \tag{17}$$

D. Quarter- and Half-Wave Symmetry With Unipolar Switch Positions

In the traditional unipolar OPP problem formulation, the switch positions are required to be non-negative in the positive half-wave of the fundamental period. Together with the requirement that the initial switch position has to be zero, i.e., $u_0 = 0$, the switching transitions directly follow to $\Delta u_i = (-1)^{1+i} \;\; \forall\, i \in \{1, \ldots, d\}$ for three-level pulse patterns. Thus, the sequence of switch positions becomes $u_s = [0\ 1\ 0\ 1 \ldots]^T$, which eliminates the switch positions as optimization variables.

TABLE II
SYSTEM PARAMETER FOR OPP COMPUTATION

Parameter	Symbol	SI value
Rated line-to-line voltage	V_R	3.3 kV
Rated stator current	I_R	2.12 kA
Rated angular stator frequency	ω_{sR}	$2\pi 50$ rad/s
Dc-link voltage	V_{dc}	5.2 kV
Total leakage inductance	L_σ	0.73 mH

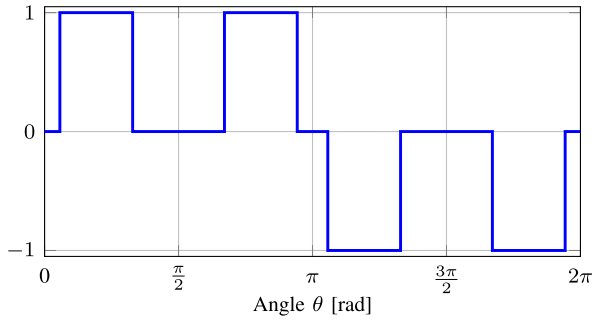

Fig. 3. QaHWS pulse patterns with $d = 2$, $m = 0.6$ and unipolar switch positions.

For the traditional OPP problem, the switching angles in the first quarter of the fundamental period remain as optimization variables $\alpha_s = [\alpha_1 \ldots \alpha_d]^T$. The resulting optimization problem is as follows

$$\begin{aligned} \underset{\alpha_s}{\text{minimize}} \quad & J(\alpha_s) = \sum_{n=5,7,11,\ldots} \left(\frac{b_n}{n}\right)^2 \\ \text{subject to} \quad & b_1 = m \\ & 0 \le \alpha_1 \le \alpha_2 \le \ldots \le \alpha_d \le \frac{\pi}{2}. \end{aligned} \tag{18}$$

V. OPP COMPUTATION

OPPs resulting from all four previously formulated optimization problems are computed for a three-level neutral-point-clamped inverter connected to a three-phase medium-voltage induction machine. The system parameters are given in Table II. In a per unit system (pu) based on the rated values in this table, the induction machine has a total leakage inductance of $X_\sigma = 0.255\,\text{pu}$. For the computation, the `fmincon` solver of MATLAB was used.

Modulation indices in the range from 0 to $\frac{4}{\pi}$ with a step size of 0.01 were considered. At each modulation index, each optimization problem was solved for 100 random initial conditions, which increases the probability of finding the global minimum. The infinite sum of harmonics in the objective function was approximated by considering the first 100 harmonics. This can be justified by the fact that the amplitudes of the harmonic currents are very small at high frequencies.

In the multipolar optimization problems (15), (16), and (17), the switching angles α_i and the switch positions u_i are the optimization variables. Due to the restriction of the switch positions to integer values, these problems are mixed-integer

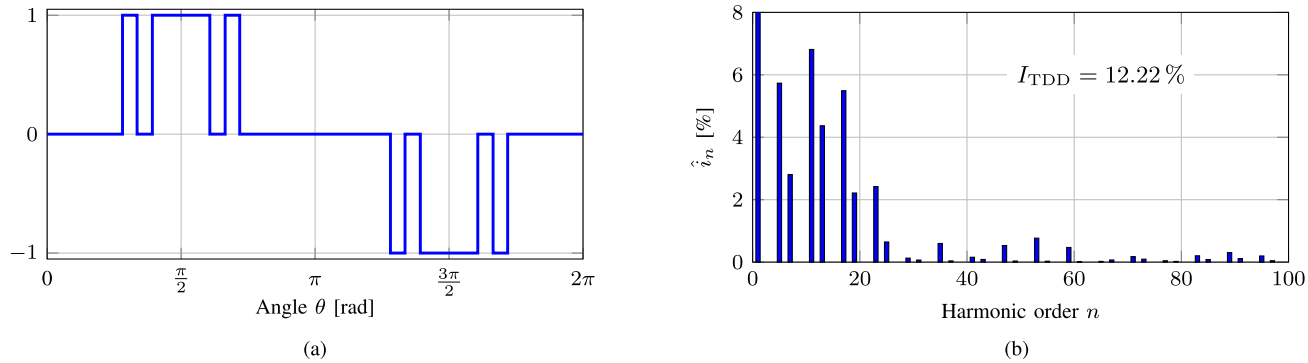

Fig. 4. (a) Pulse pattern and (b) harmonic current spectrum of the QaHWS OPP with $d = 3$, $m = 0.6$ and unipolar switch positions $u_i \in \{0, 1\}, \forall i \in \{1, \ldots, d\}$.

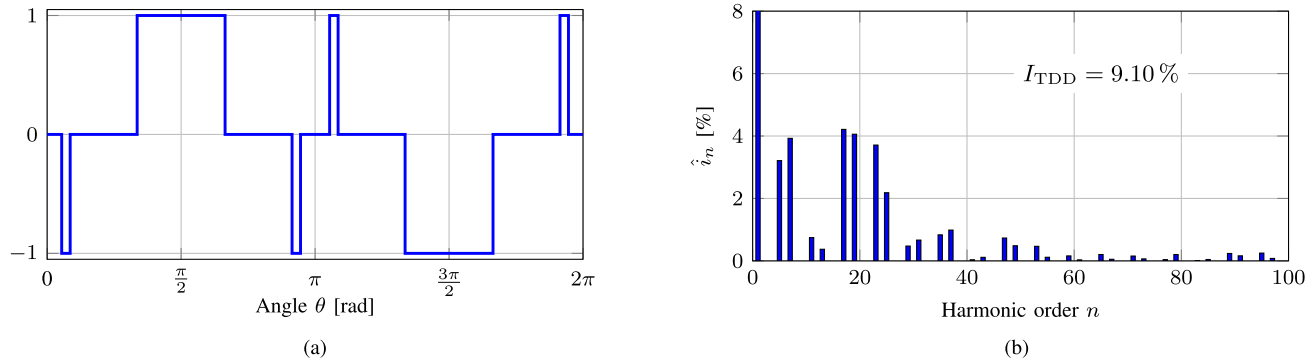

Fig. 5. (a) Pulse pattern and (b) harmonic current spectrum of the QaHWS OPP with $d = 3$, $m = 0.6$ and multipolar switch positions $u_i \in \{-1, 0, 1\}, \forall i \in \{1, \ldots, d\}$.

optimization problems. For a small number of switching angles, it is a common practice to enumerate all feasible sequences of switch positions (switching sequences) [18]. For each switching sequence, the optimization problem reduces to a nonlinear optimization problem with the switching angles as optimization variables.[2]

OPPs with pulse numbers 2 and 3 were computed for all four optimization problems. For the FWS problem, also the noninteger pulse numbers 1.5 and 2.5 were considered.

A. Quarter- and Half-Wave Symmetric (QaHWS) Optimized Pulse Patterns

We consider an OPP with quarter- and half-wave symmetry and pulse number 2, as shown in Fig. 3. Recall that the fundamental component of the pulse pattern has to have zero phase shift. When allowing multipolar switch positions, the second switch position u_1 becomes an optimization variable. This leads to two possible switching sequences. When choosing $u_1 = -1$, all switch positions in the positive half-wave of the fundamental period are negative. This corresponds to a phase shift of 180° of the fundamental component, which makes the optimization problem infeasible. Therefore, the only feasible switching sequence for the multipolar, QaHWS OPP with pulse number 2 is the traditional switching sequence with unipolar switch positions, as shown in Fig. 3. Consequently, this results in the well-known traditional OPP.

For higher pulse numbers, e.g., pulse number 3, and when allowing multipolar switch positions, several feasible switching sequences for QaHWS OPPs arise. Besides the traditional OPP with unipolar switch positions, as shown in Fig. 4(a), one example of a multipolar switching sequence is shown in Fig. 5(a). The amplitudes of the corresponding current harmonics up to the 50th order are shown in Figs. 4(b) and 5(b). In this example with modulation index $m = 0.6$, the optimal solution is the multipolar OPP, which reduces the current TDD by 25% relative to the current TDD of the traditional unipolar OPP. The low-order harmonics are particularly reduced, whereas harmonics of higher order are slightly increased.

Considering the entire modulation range, the current TDDs of the two QaHWS OPPs are compared in Fig. 6. Allowing multipolar switch positions reduces the current TDD in the highlighted interval of modulation indices. In Table III, the range of modulation indices for which the current TDD can be reduced, and the maximum absolute and relative reductions of the current TDD within this interval are listed. Note that in the remainder of

[2]A generalized formulation of the optimization problem for multilevel OPPs was presented in [19]. The two sets of optimization variables are combined into a single set, which reduces the mixed-integer problem again to a nonlinear optimization problem. However, this approach is based on the assumption of quarter- and half-wave symmetry and, thus, not directly applicable to optimization problems with half-wave and full-wave symmetry. For the SHE formulation with half-wave symmetry, a similar approach of virtual firing angles was presented in [20].

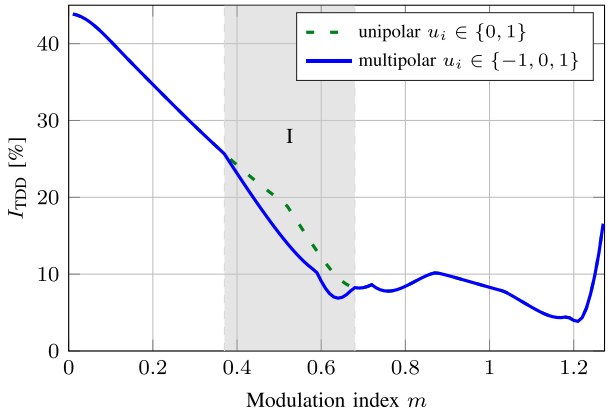

Fig. 6. Current TDDs of QaHWS OPPs with $d = 3$.

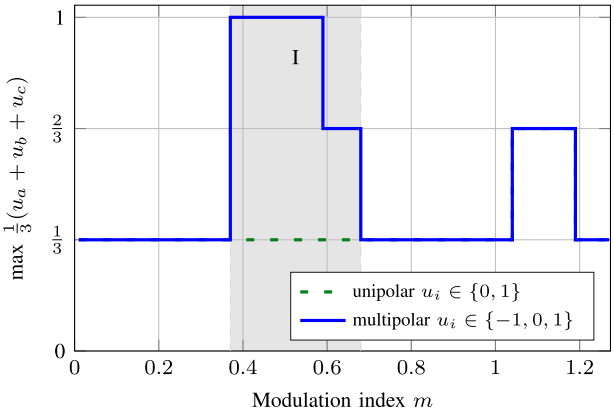

Fig. 7. Maximum common-mode switch positions of QaHWS OPPs with $d = 3$.

TABLE III
INTERVALS OF CURRENT TDD REDUCTION WHEN ALLOWING MULTIPOLAR SWITCH POSITIONS FOR QAHWS OPPS WITH $d = 3$

Interval	Modulation index interval	Maximum absolute reduction of current TDD	Maximum relative reduction of current TDD
I	$0.37 \leq m \leq 0.67$	4.83 %	30.68 %

the modulation range, the unipolar and the multipolar problem formulations yield the same OPPs.

Another important metric is the common-mode switch position of an OPP. The common-mode switch position is the sum of the three single-phase switching signals $u_x = \frac{1}{3}(u_a + u_b + u_c)$, where u_a, u_b, and u_c are the switching signals in the phases a, b, and c, respectively. The common-mode voltage can be directly calculated from the common-mode switch position with $v_x = \frac{V_{\mathrm{dc}}}{2} u_x$. We consider the maximum common-mode switch position over a fundamental period of both OPPs in Fig. 7 for the entire modulation range. The multipolar OPP reduces the current TDD in Interval I, but increases the maximum common-mode voltage by up to three times. This is clearly a disadvantage, and such OPPs might not be suitable for some loads. Alternatively, the common-mode switch position could be limited to $\frac{2}{3}$, at the expense of a slightly higher current TDD.

B. Half-Wave Symmetric Optimized Pulse Patterns

Relaxing quarter-wave symmetry and allowing multipolar switch positions increases the search space of the three-level OPP problem in two ways. First, the domain of the switching angles increases, which allows the optimization variables to vary within one half-wave of the fundamental period, i.e., $\alpha_i \in [0, \pi]$. Compared with the traditional OPP solutions, this means that switching angles can be shifted beyond $\frac{\pi}{2}$. Examples of such HWS OPPs are shown in Fig. 8 for pulse numbers 2 and 3. We can see that in both OPPs, more than half the switching angles in one half-wave occur in one quarter of the fundamental period. This results in new optimal solutions, which reduce the current TDD by up to 19% relative to the QaHWS OPPs for pulse number 2.

The search space is further increased in HWS OPPs by turning the initial switch position into an additional optimization variable with $u_0 \in \{-1, 0, 1\}$. This gives rise to additional feasible switching sequences, even for pulse number 2. Examples for OPPs with these multipolar switching sequences are shown in Fig. 9.

The modulation index of the HWS OPP with pulse number 3 in Fig. 9(b) matches that of the multipolar OPP with quarter- and half-wave symmetry in Fig. 5(a). This facilitates a direct comparison of the two OPPs. While the QaHWS OPP has two negative pulses in the positive half-wave of the fundamental period, the HWS OPP switches only once to the negative level in the positive half-wave. The latter reduces the current TDD by another 5.31% relative to the current TDD of the multipolar QaHWS OPP.

Consider again the entire modulation range. In Fig. 10, the current TDDs of HWS OPPs are compared with those of QaHWS OPPs. This is done for pulse numbers 2 and 3. The figure shows that for both pulse numbers, the HWS solutions reduce the current TDD in three intervals of the modulation range. For the remaining modulation indices, the solutions correspond to the traditional QaHWS OPPs. The corresponding ranges of modulation indices for which the current TDD is improved, and the maximum absolute and relative improvements of the current TDD within these intervals are listed in Table IV for pulse number 2 and in Table V for pulse number 3.

For both pulse numbers, the lower current TDDs in Interval I are exclusively achieved by OPPs with multipolar switch positions such as the OPPs in Fig. 9. In Intervals II and III, OPPs with unipolar switch positions and shifted switching angles, such as the OPPs in Fig. 8, lead to the reductions of the current TDD.

Fig. 11 shows the switching angles in the first half-wave (from 0 to π) of the HWS OPP with pulse number 2. The Intervals I, II, and III correspond to the respective intervals in Fig. 10(a). Within these intervals, quarter-wave symmetry is abandoned. In particular, within Intervals II and III, the third angle α_3 is moved into the first quarter-wave. Outside of these three intervals, quarter-wave symmetry arises, because it minimizes the current distortions and not because it was imposed.

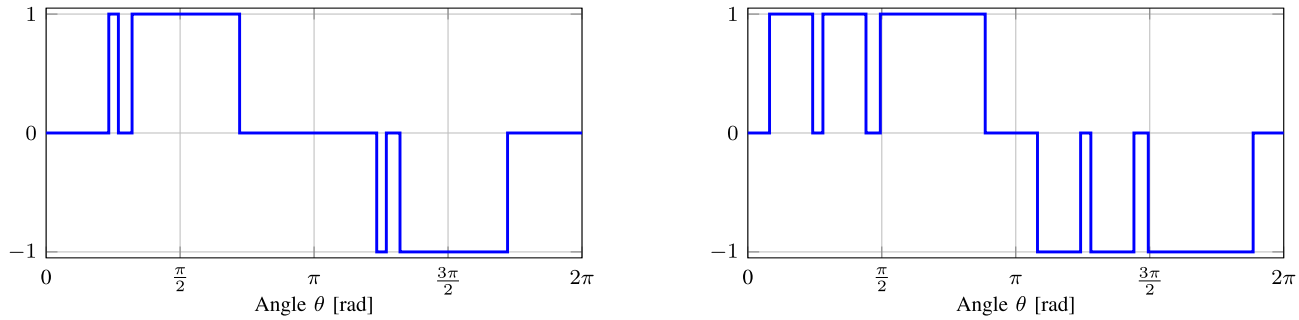

Fig. 8. HWS OPP with (a) $d = 2$ and $m = 0.8$, and with (b) $d = 3$ and $m = 1.05$ with unipolar switch positions and shifted switching angles.

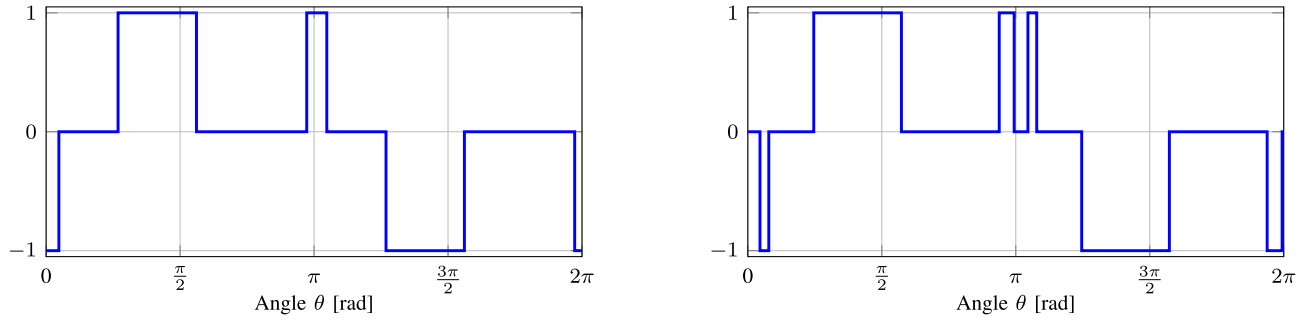

Fig. 9. HWS OPP with (a) $d = 2$ and $m = 0.54$, and with (b) $d = 3$ and $m = 0.6$ with multipolar switch positions.

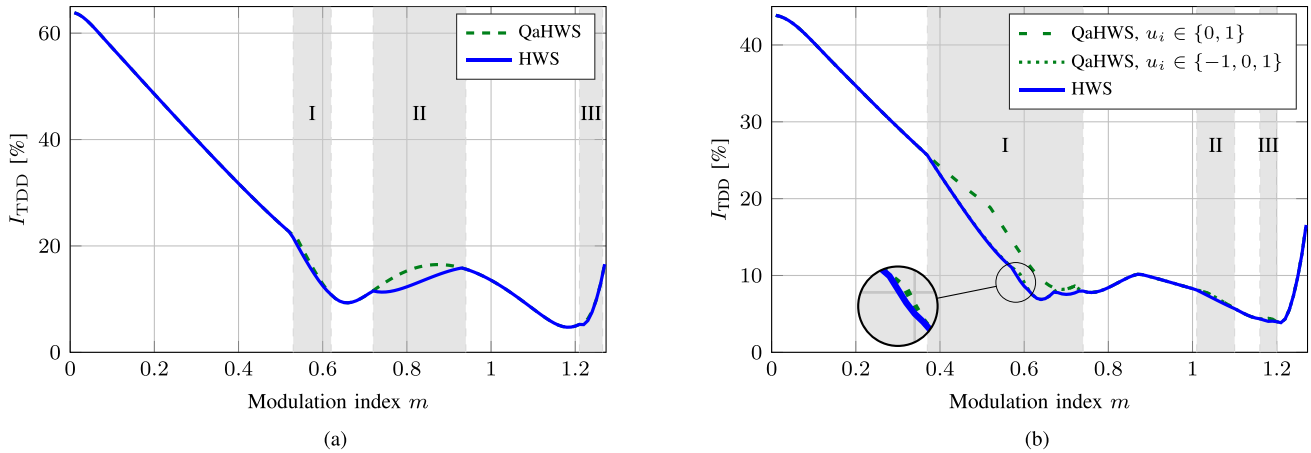

Fig. 10. Current TDDs of HWS and QaHWS OPPs compared for (a) pulse number $d = 2$ and (b) pulse number $d = 3$.

TABLE IV
INTERVALS OF CURRENT TDD IMPROVEMENT WHEN RELAXING QUARTER-WAVE SYMMETRY FOR $d = 2$

Interval	Modulation index interval	Maximum absolute reduction of current TDD	Maximum relative reduction of current TDD
I	$0.53 \leq m \leq 0.61$	1.20 %	5.64 %
II	$0.72 \leq m \leq 0.93$	2.99 %	19.52 %
III	$1.22 \leq m \leq 1.26$	0.490 %	8.60 %

TABLE V
INTERVALS OF CURRENT TDD IMPROVEMENT WHEN RELAXING QUARTER-WAVE SYMMETRY FOR $d = 3$

Interval	Modulation index interval	Maximum absolute reduction of current TDD	Maximum relative reduction of current TDD
I	$0.37 \leq m \leq 0.73$	4.91 %	30.68 %
II	$1.01 \leq m \leq 1.10$	0.331 %	4.35 %
III	$1.17 \leq m \leq 1.19$	0.383 %	8.67 %

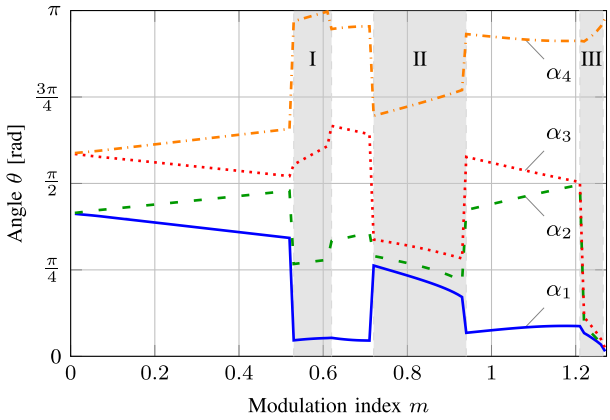

Fig. 11. Switching angles for the HWS OPP with pulse number $d = 2$.

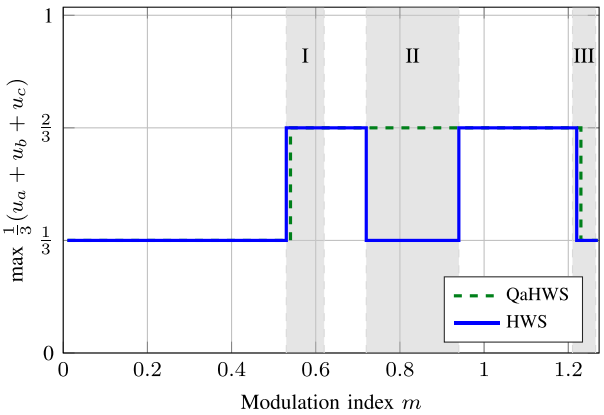

Fig. 12. Maximum common-mode switch positions of HWS and QaHWS OPPs for pulse number $d = 2$.

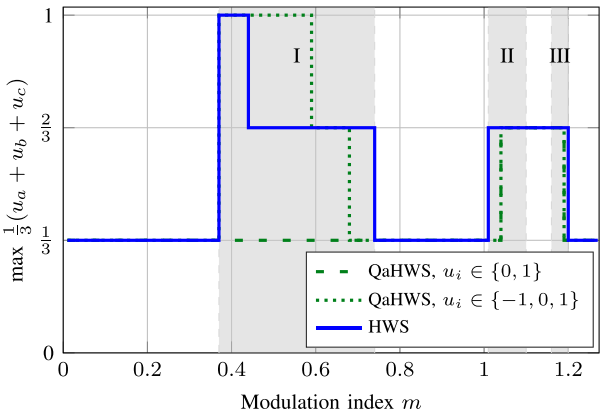

Fig. 13. Maximum common-mode switch positions of HWS and QaHWS OPPs for pulse number $d = 3$.

The maximum common-mode switch positions resulting from the HWS OPPs with pulse numbers 2 and 3 are shown in Fig. 12 and Fig. 13 over the entire modulation range. The respective intervals of current TDD reductions are also indicated in these figures. We can see from Fig. 12 that for pulse number 2, the maximum common-mode switch position never exceeds $\frac{2}{3}$.

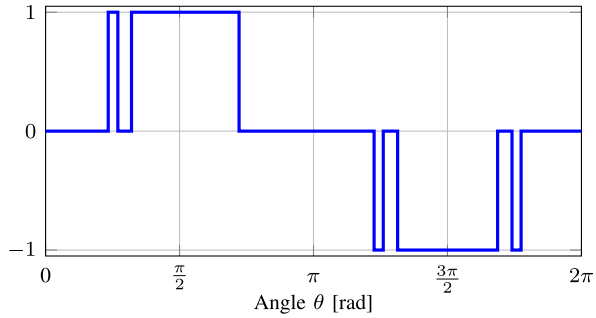

Fig. 14. FWS OPP with pulse number $d = 2.5$ and $m = 0.8$.

Moreover, in Interval II, the OPP with shifted switching angles reduces the maximum common-mode switch position. This means that for pulse number 2 OPPs with relaxed quarter-wave symmetry achieve a superior performance in terms of current TDD *and* common-mode voltage.

For pulse number 3, we can observe a similar behavior in the maximum common-mode switch position from Fig. 13. Recall that the current TDD reduction in Interval I, which is achieved by the QaHWS OPP with multipolar switch positions, entails an increase in the common-mode voltage. In comparison, the HWS OPP with multipolar switch positions achieves a reduction of the common-mode voltage in this interval. Thus, we conclude for pulse number 3 that relaxing quarter-wave symmetry lowers the current TDD and partly mitigates the adverse increase in the common-mode voltage.

C. *Full-Wave Symmetric Optimized Pulse Patterns*

Last, we consider the optimization problem of FWS OPPs. Interestingly, at least for pulse numbers 2 and 3, the resulting switching patterns exhibit half-wave symmetry; imposing half-wave symmetry, therefore, has no adverse effect on the optimality of OPPs. However, it halves the number of optimization variables and, therefore, shortens the computation time.

As stated in Section IV, full-wave symmetry gives rise to OPPs with noninteger pulse numbers. An example of such an OPP with pulse number $d = 2.5$ is shown in Fig. 14. Even though this OPP constitutes an entirely new pulse pattern, close inspection of the two individual half-waves reveals that the pattern is the combination of two HWS OPPs: one with pulse number 2 from 0 to π [see Fig. 8(a)], and another one with pulse number 3 from π to 2π. Another OPP with the same current distortions exists, where the first half-wave corresponds to the OPP with pulse number 3 and the second one to the HWS OPP with pulse number 2.

This characteristic has also been observed for other modulation indices and noninteger pulse numbers. More specifically, the two half-waves of an FWS OPP with the noninteger pulse number d appear to correspond to the half-waves of two OPPs with half-wave symmetry: one with integer pulse number $\lfloor d \rfloor$, and another one with integer pulse number $\lceil d \rceil$. Note that $\lfloor d \rfloor$ and $\lceil d \rceil$ refer to the *floor* and *ceiling* operation, respectively, rounding d to the smaller and larger integer.

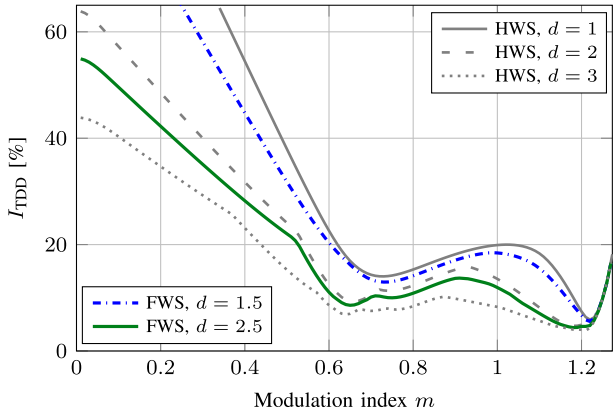

Fig. 15. Current TDDs of FWS OPPs with noninteger pulse numbers and HWS OPPs with integer pulse numbers.

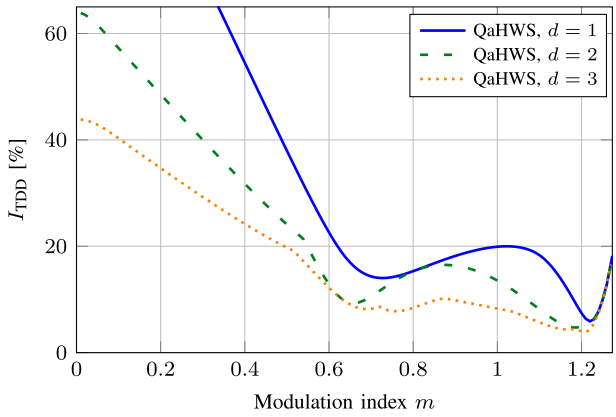

Fig. 16. Current TDDs of the traditional unipolar QaHWS OPPs.

Fig. 15 shows the current TDDs of the FWS OPPs with pulse numbers 1.5 and 2.5 together with those of the HWS OPPs with integer pulse numbers over the entire modulation range. We can see that for each modulation index, the OPPs with noninteger pulse numbers yield significantly different current TDDs than those with integer pulse numbers. More specifically, the current TDDs of OPPs with noninteger pulse number are bounded from above and below by those of OPPs with floor- and ceil-rounded integer pulse numbers. This is in line with the earlier observation that OPPs with noninteger pulse numbers d are the combination of OPPs with pulse numbers $\lfloor d \rfloor$ and $\lceil d \rceil$.

In Fig. 16, the current TDDs of the traditional, unipolar QaHWS OPPs are shown for the integer pulse numbers 1, 2, and 3. The figure shows that at certain modulation indices, the current TDD of the higher pulse number equals that of the smaller one. At $m = 0.8$, for example, the current TDDs of the OPPs with pulse numbers 1 and 2 are both 15.3%. When relaxing symmetry and allowing multipolar switch positions, we observe from Fig. 15 that at each modulation index, there is a considerable reduction in the current TDD when increasing the pulse number.

VI. Experimental Results

The results in Section V are verified with a small-scale experimental setup. The setup consists of a squirrel-cage induction machine, with its parameters shown in Table VI, and three Infineon F3L030E07 evaluation boards each fitted with an F3L75R07W2E3 three-level IGBT module. The OPPs are stored in lookup tables on a field-programmable gate array.

TABLE VI
Machine Parameter of the Experimental Setup

Parameter	Symbol	SI value
Rated line-to-line voltage	V_R	380 V
Rated stator current	I_R	12.1 A
Rated angular stator frequency	ω_{sR}	$2\pi 50$ rad/s

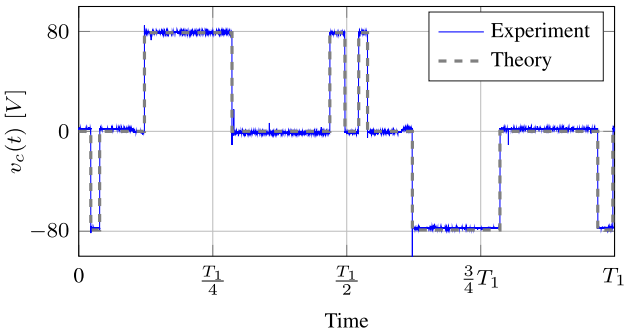

Fig. 17. Inverter phase voltage with $d = 3$ and $m = 0.6$.

To ensure a proper analysis, the neutral point of the NPC converter is required to be fixed to zero. This can easily be achieved by using two power supplies; one for each half of the dc-link voltage. However, the power supplies available for the experimental setup limit the dc-link voltage to $V_{\text{dc}} = 160$ V. A load is added to the machine with equal torque in all measurements. The rated parameters of the machine are used as base values for the per unit system.

The inverter is operated at the operating points of the four OPPs shown in Figs. 8 and 9. At each operating point, the phase voltage and current are measured when applying, first, the traditional QaHWS OPP and, second, the HWS OPP. For example, the waveforms of the measured and theoretical phase voltages resulting from the HWS OPP with $d = 3$ and $m = 0.6$ are shown in Fig. 17.

From the measured inverter phase current, the harmonic amplitudes are computed and the current TDD is calculated. The current harmonics resulting from the traditional QaHWS OPP with $d = 3$ and $m = 0.6$ are shown in Fig. 18. At the same operating point, the theoretically computed current spectrum is shown in Fig. 4(b). Note that due to the low dc-link voltage and different leakage inductance in the experimental setup, different values for the current harmonics result. However, inspection of the two figures reveals a similar profile of the harmonic spectra. The noise in the experimental results is caused by nonidealities in the setup. Additionally, the current harmonics from the experimental calculations may differ from the theory due to the neglected stator resistance in the theoretical calculations.

The reduction of the current distortions by the proposed relaxed OPPs can be observed by comparing Fig. 18 with Fig. 19. The latter shows the harmonic spectrum of the

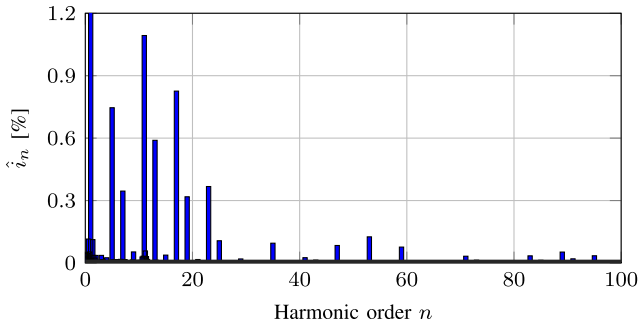

Fig. 18. Experimentally obtained current harmonic spectrum of the QaHWS OPP with $d = 3$ and $m = 0.6$.

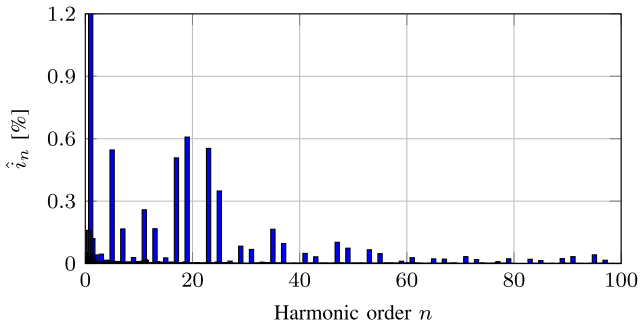

Fig. 19. Experimentally obtained current harmonic spectrum of the HWS OPP with $d = 3$ and $m = 0.6$.

TABLE VII
COMPARISON OF THE CURRENT TDDS IN THEORY AND CALCULATED FROM THE EXPERIMENTAL MEASUREMENTS AT FOUR OPERATING POINTS

Operating Point	Theory		Experiment	
	QaHWS	HWS	QaHWS	HWS
$d = 2$, $m = 0.54$	21.28 %	20.16 %	2.76 %	2.69 %
$d = 2$, $m = 0.8$	15.31 %	12.27 %	2.23 %	1.79 %
$d = 3$, $m = 0.6$	12.22 %	8.66 %	1.81 %	1.28 %
$d = 3$, $m = 1.05$	7.30 %	7.03 %	1.25 %	1.22 %

phase current resulting from the HWS OPP with $d = 3$ and $m = 0.6$, which results in a significant reduction of the 11th and 13th harmonics.

The current TDDs obtained from all eight OPPs, the traditional and relaxed OPPs at the four operating points, are summarized in Table VII and compared with the theoretical results. In all four operating points, a similar reduction of the current TDD is achieved by the HWS OPPs, which verifies the theory.

VII. CONCLUSION

Quarter- and half-wave symmetry and unipolar switch positions are universally imposed when computing three-level OPPs, limiting the search space within which the "optimal" switching pattern can be found. This article has shown that these restrictions lead, in general, to suboptimal solutions. By relaxing quarter-wave symmetry and by considering multipolar switch positions, OPPs with lower harmonic distortions can be found.

More specifically, OPPs with pulse number 2 and half-wave symmetry reduce the current distortions by up to 20%, when compared to traditional OPPs with quarter- and half-wave symmetry. Besides the relaxation of quarter-wave symmetry, the somewhat artificial restriction of unipolar switch positions can be removed for OPPs with pulse number 3; by allowing also negative switch positions in the positive half-wave of the fundamental period, the switch positions are included in the optimization problem. This reduces the current distortions by up to 31% for pulse number 3. These results are verified with a small-scale experimental setup.

REFERENCES

[1] A. Edpuganti and A. K. Rathore, "A survey of low switching frequency modulation techniques for medium-voltage multilevel converters," *IEEE Trans. Ind. Appl.*, vol. 51, no. 5, pp. 4212–4228, Sep. 2015.
[2] F. G. Turnbull, "Selected harmonic reduction in static D-C–A-C inverters," *IEEE Trans. Commun. Electron.*, vol. CE-83, no. 73, pp. 374–378, Jul. 1964.
[3] H. S. Patel and R. G. Hoft, "Generalized techniques of harmonic elimination and voltage control in thyristor inverters: Part I–Harmonic elimination," *IEEE Trans. Ind. Appl.*, vol. IA-9, no. 3, pp. 310–317, May 1973.
[4] H. S. Patel and R. G. Hoft, "Generalized techniques of harmonic elimination and voltage control in thyristor inverters: Part II–Voltage Control Techniques," *IEEE Trans. Ind. Appl.*, vol. IA-10, no. 5, pp. 666–673, Sep. 1974.
[5] J. N. Chiasson, L. M. Tolbert, K. J. McKenzie, and Z. Du, "A unified approach to solving the harmonic elimination equations in multilevel converters," *IEEE Trans. Power Electron.*, vol. 19, no. 2, pp. 478–490, Mar. 2004.
[6] G. S. Buja and G. B. Indri, "Optimal pulsewidth modulation for feeding AC motors," *IEEE Trans. Ind. Appl.*, vol. IA-13, no. 1, pp. 38–44, Jan. 1977.
[7] G. S. Buja, "Optimum output waveforms in PWM inverters," *IEEE Trans. Ind. Appl.*, vol. IA-16, no. 6, pp. 830–836, Nov. 1980.
[8] J. A. Pontt, J. R. Rodriguez, A. Liendo, P. Newman, J. Holtz, and J. M. S. Martin, "Network-friendly low-switching-frequency multipulse high-power three-level PWM rectifier," *IEEE Trans. Ind. Electron.*, vol. 56, no. 4, pp. 1254–1262, Apr. 2009.
[9] A. K. Rathore, J. Holtz, and T. Boller, "Generalized optimal pulsewidth modulation of multilevel inverters for low-switching-frequency control of medium-voltage high-power industrial ac drives," *IEEE Trans. Ind. Electron.*, vol. 60, no. 10, pp. 4215–4224, Oct. 2013.
[10] J. R. Wells, B. M. Nee, P. L. Chapman, and P. T. Krein, "Selective harmonic control: a general problem formulation and selected solutions," *IEEE Trans. Power Electron.*, vol. 20, no. 6, pp. 1337–1345, Nov. 2005.
[11] M. S. A. Dahidah, G. Konstantinou, N. Flourentzou, and V. G. Agelidis, "On comparing the symmetrical and non-symmetrical selective harmonic elimination pulse-width modulation technique for two-level three-phase voltage source converters," *IET Power Electron.*, vol. 3, no. 6, pp. 829–842, Nov. 2010.
[12] J. R. Wells, P. L. Chapman, and P. T. Krein, "Generalization of selective harmonic control/elimination," in *Proc. IEEE 36th Power Electron. Spec. Conf.*, Jun. 2005, pp. 1358–1363.
[13] A. Tripathi and G. Narayanan, "Optimal pulse width modulation of voltage-source inverter fed motor drives with relaxation of quarter wave symmetry condition," in *Proc. IEEE Int. Conf. Electron., Comput. Commun. Technol.*, Jan. 2014, pp. 1–6.
[14] A. Tripathi and G. Narayanan, "High-performance off-line pulse width modulation without quarter wave symmetry for voltage-source inverter," in *Proc. Int. Conf. Adv. Electron. Comput. Commun.*, Oct. 2014, pp. 1–6.
[15] A. D. Birda, J. Reuss, and C. Hackl, "Synchronous optimal pulse-width modulation with differently modulated waveform symmetry properties for feeding synchronous motor with high magnetic anisotropy," in *Proc. Euro. Conf. Power Electron. Appl.*, Sep. 2017, pp. P.1–P.10.
[16] G. Scheuer, "Investigation of the 3-level voltage source inverter (VSI) for flexible AC-transmission systems (FACTS) exemplified on a static var compensator (SVC)," Ph.D. dissertation, ETH Zurich, Zurich, Switzerland, 1997.
[17] T. Geyer, *Model Predictive Control of High Power Converters and Industrial Drives*. New York, NY, USA: Wiley, 2016.

[18] A. K. Rathore, J. Holtz, and T. Boller, "Synchronous optimal pulsewidth modulation for low-switching-frequency control of medium-voltage multilevel inverters," *IEEE Trans. Ind. Electron.*, vol. 57, no. 7, pp. 2374–2381, Jul. 2010.
[19] J. Lago and M. L. Heldwein, "Generalized synchronous optimal pulse width modulation for multilevel inverters," *IEEE Trans. Power Electron.*, vol. 32, no. 8, pp. 6297–6307, Aug. 2017.
[20] A. Prez-Basante, S. Ceballos, G. Konstantinou, J. Pou, I. Kortabarria, and I. M. de Alegra, "A universal formulation for multilevel selective-harmonic-eliminated PWM with half-wave symmetry," *IEEE Trans. Power Electron.*, vol. 34, no. 1, pp. 943–957, Jan. 2019.

Annika Birth (S'19) received the B.Sc. degree in electrical engineering from the University of Applied Sciences Stralsund, Stralsund, Germany, in 2017. She is currently working toward the M.Eng. degree in electrical engineering with the Stellenbosch University, Stellenbosch, South Africa, which is in collaboration with ABBs Corporate Research Centre, Baden-Dättwil, Switzerland.

Her research interests include optimized pulse patterns and model predictive control for medium-voltage drives.

Tobias Geyer (M'08–SM'10) received the Dipl.-Ing. and Ph.D. degrees in electrical engineering from ETH Zurich, Zurich, Switzerland, in 2000 and 2005, respectively, and the Habilitation degree in power electronics from ETH Zurich, Zurich, Switzerland, in 2017.

After his Ph.D., he spent three years at GE Global Research, Munich, Germany, and another three years at the University of Auckland, Auckland, New Zealand. In 2012, he joined ABBs Corporate Research Centre, Baden-Dättwil, Switzerland, where he is currently a Senior Principal Scientist for power conversion control. He was appointed as an extraordinary Professor with Stellenbosch University, Stellenbosch, South Africa, from 2017 to 2020. He is the author of more than 130 peer-reviewed publications, 30 patent applications, and the book *Model predictive control of high power converters and industrial drives* (Wiley, 2016). He teaches a regular course on model predictive control at ETH Zurich. His research interests include medium-voltage and low-voltage drives, utility-scale power converters, and model predictive control.

Dr. Geyer received the 2017 First Place Prize Paper Award in the *Transactions on Power Electronics*, the 2014 Third Place Prize Paper Award in the *Transactions on Industry Applications*, and two prize paper awards at conferences. He is a former Associate Editor for the *Transactions on Industry Applications* (from 2011 until 2014) and the *Transactions on Power Electronics* (from 2013 until 2019). He was an International Program Committee Vice Chair of the IFAC Conference on Nonlinear Model Predictive Control in Madison, WI, USA, in 2018.

Hendrik du Toit Mouton (S'98–M'00) received the B.Sc., B.Sc.Hons, M.Sc., and Ph.D. degrees in mathematics degrees from the University of the Orange Free-state, Bloemfontein, South Africa, in 1986, 1987, 1988, and 1991, respectively and the B.Eng. and Ph.D. degrees in electrical engineering from the Stellenbosch University, Stellenbosch, South Africa, in 1996 and 2000, respectively.

He is currently a Professor in electrical engineering with Stellenbosch University, and also Leader of the Power Electronics Research Group. He has authored and coauthored more than 130 journal and conference papers in mathematics and power electronics.

His research interests include multilevel converters, modelling and control of power electronic converters, and class-D audio amplifiers.

Martinus Dorfling (S'19) received the B.Eng. degree in electrical and electronic engineering and the M.Eng. degree in electrical engineering from the Stellenbosch University, Stellenbosch, South Africa, in 2015 and 2018, respectively, where he is currently working towards the Ph.D. degree in electrical engineering.

His research interests include optimized pulse patterns, model predictive control, and the implementation of control algorithms on field programmable gate arrays.